

Article

Slow Magnetic Relaxation in Cobalt(II) Complexes with One-Dimensional Hydrogen-Bonded Networks

Ryoji Mitsuhashi ^{1,*}, Hiroshi Sakiyama ² and Yoshihito Hayashi ³¹ Institute of Liberal Arts and Science, Kanazawa University, Kakuma, Kanazawa 920-1192, Japan² Department of Science, Faculty of Science, Yamagata University, 1-4-12 Kojirakawa, Yamagata 990-8560, Japan³ Department of Chemistry, Kanazawa University, Kakuma, Kanazawa 920-1192, Japan

* Correspondence: mitsuhashi@staff.kanazawa-u.ac.jp

Abstract: Two new cobalt(II) complexes with an unsymmetrical bidentate ligand, 2-(1,4,5,6-tetrahydro pyrimidin-2-yl)-6-methoxyphenol (H₂mthp), were synthesized and crystallographically characterized. Tetra- and hexa-coordinate mononuclear complexes were selectively obtained by adjusting the stoichiometry of the base. The coordination geometry of hexa-coordinated complex was severely distorted from an ideal octahedron, due to the NO₅ coordination environment from the mixed coordination of one Hmthp[−] and two H₂mthp ligands. Both complexes formed one-dimensional chain networks by hydrogen-bond and N-H⋯π interactions. Single-molecule magnet behavior was observed for the tetrahedral complex under zero magnetic field. The relatively short Co⋯Co distances induced non-zero intermolecular magnetic coupling, which split the ground $\pm M_s$ levels to suppress quantum-tunneling of magnetization. In the octahedral complex, by contrast, the distance was not short enough to induce the coupling. As a consequence, single-molecule magnetic behavior was observed for the octahedral complex only in the presence of an external static field.

Keywords: cobalt(II) complex; hydrogen-bonding interactions; single-ion magnet



Citation: Mitsuhashi, R.; Sakiyama, H.; Hayashi, Y. Slow Magnetic Relaxation in Cobalt(II) Complexes with One-Dimensional Hydrogen-Bonded Networks. *Magnetochemistry* **2023**, *9*, 17. <https://doi.org/10.3390/magnetochemistry9010017>

Academic Editor: Salah Massoud

Received: 28 November 2022

Revised: 28 December 2022

Accepted: 30 December 2022

Published: 1 January 2023

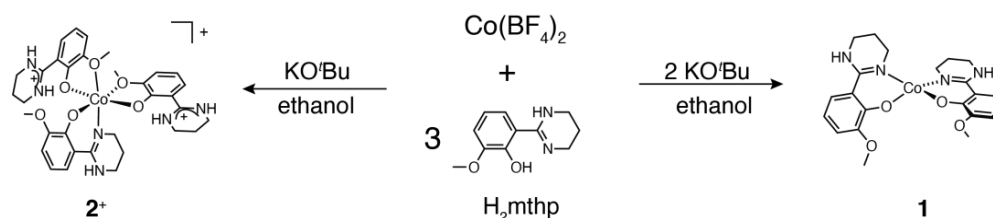


Copyright: © 2023 by the authors. Licensee MDPI, Basel, Switzerland. This article is an open access article distributed under the terms and conditions of the Creative Commons Attribution (CC BY) license (<https://creativecommons.org/licenses/by/4.0/>).

1. Introduction

Single-molecule magnets (SMMs) [1] are of considerable current interest due to their potential applications in high-density storage, spintronics and quantum computing [2–5]. To exhibit slow relaxation of magnetization, a bistable spin ground state with a large negative axial zero-field splitting (ZFS) is important because the spin-reversal barrier U is proportionally dependent on the axial ZFS parameter D , where $U = |D|S^2$ for an integer spin system and $|D|(S^2 - 1/4)$ for a half-integer spin system). SMMs with a single paramagnetic center are called single-ion magnets (SIMs) [6]. Owing to the simplicity and facile design of the molecule, many lanthanide and first-row transition metal complexes have been studied to prepare SMMs with a strong magnetic anisotropy [7–13]. Cobalt(II) complexes are one of the most studied metal ions as SIMs because tetra- and hexa-coordinated cobalt(II) complexes often exhibit strong magnetic anisotropy [8–17]. In most of the examples of 3d metal-based SIMs, however, slow magnetic relaxation was not observed in the absence of an external magnetic field, due to fast relaxation via quantum-tunneling of magnetization (QTM). For a Kramers ion, QTM arises from the mixing of $\pm M_s$ level hyperfine or dipolar interactions [11]. Avoiding a close interaction between SMMs in the long distance is one of the possible solutions to avoid the QTM phenomena by dipolar interactions. On the other hand, we recently reported zero-field SIM behaviors in tetrahedral cobalt(II) complexes with one-dimensional hydrogen-bonded networks [12,13]. It is suggested that relatively short intermolecular distances (ca. 6 Å) and one-dimensional alignments of the complexes suppress the QTM by splitting the ground $\pm M_s$ levels by intermolecular magnetic coupling [18–21]. However, the correlation between intermolecular distances and the alignments of the SMMs within the chain structure remain unclear. In this

paper, we synthesized an analogous tetrahedral cobalt(II) complex and a severely distorted octahedral cobalt(II) complex with one-dimensional networks (Scheme 1). The effects of intrachain distances and alignments of SIMs on QTM phenomena were investigated, and zero-field and field-induced SIM behaviors were observed in tetrahedral and octahedral complexes, respectively.



Scheme 1. Chemical structures and preparation schemes of a tetrahedral and octahedral cobalt(II) complexes **1** and 2^+ .

2. Results and Discussion

2.1. Preparation of the Ligand and Cobalt(II) Complexes

The ligand precursor 2-(1,4,5,6-tetrahydropyrimidin-2-yl)-6-methoxyphenol (H_2mthp) was prepared by a similar method to that reported for an analogous ligand in the literature [13]. The mononuclear bis-bidentate type complex $[\text{Co}(\text{Hmthp})_2] \cdot \text{C}_2\text{H}_5\text{OH}$ was synthesized by a reaction of $\text{Co}(\text{BF}_4)_2 \cdot 6\text{H}_2\text{O}$, H_2mthp and KO^tBu in 1:3:2 ratio in ethanol (Scheme 1). An excessive amount of the ligand precursor was required for the synthesis to prevent the formation of $\text{Co}(\text{OH})_2$ as impurity. It should be noted that the use of other bases, such as triethylamine, was not successful, presumably because triethylamine was not strong enough to deprotonate H_2mthp . In the case of a smaller molar ratio of KO^tBu (1:3:1 ratio), a mononuclear tris-bidentate cobalt(II) complex $[\text{Co}(\text{Hmthp})(\text{H}_2\text{mthp})_2]\text{BF}_4$ (2BF_4) was obtained. Both cobalt(II) complexes tended to lose crystallinity in air by efflorescence, and solvent molecules of crystallization were substituted by water.

2.2. Crystal Structures of H_2mthp and Cobalt(II) Complexes

The ligand precursor H_2mthp was crystallized in chiral orthorhombic space group $P2_12_12_1$. In the crystal, the asymmetric unit consisted of two independent H_2mthp molecules and existed in zwitterionic form, with a deprotonated phenol group and a protonated imino group preceded in analogous compounds (Figure S1) [22]. The X-ray crystallographic analysis revealed that $1 \cdot \text{C}_2\text{H}_5\text{OH}$ and 2BF_4 were tetra-coordinated and hexa-coordinated cobalt(II) complexes, respectively (Figures 1 and 2). In $1 \cdot \text{C}_2\text{H}_5\text{OH}$, the crystallographic asymmetric unit consisted of **1** and an ethanol molecule of crystallization. The cobalt(II) ion was coordinated by phenolato-*O* and imino-*N* donors of Hmthp^- ligand in a bidentate fashion to afford a pseudo-tetrahedral coordination geometry (Table 1). The structural parameter τ_4 for **1** was calculated to be 0.77 ($\tau_4 = [360^\circ - (\alpha + \beta)]/141^\circ$, where α and β were the largest two angles in the coordination sphere), which was smaller than those of analogous complexes, indicating that the coordination geometry was more distorted from an ideal tetrahedron [23]. The mean plane angle between two bidentate ligands (O1-Co1-N2 plane to O3-Co1-N4 plane angle = 76.7°) deviated from 90° . Hydrogen-bonding interactions were observed between the N-H group of the ligand and phenolato-*O* atom of the neighboring molecule to construct one-dimensional hydrogen-bonded networks of **1**. As the crystallographic inversion centers were located between two neighboring molecules in a chain, the magnetic anisotropy axes of the molecules should be in the same axis. Two intrachain $\text{Co} \cdots \text{Co}$ distances were not equivalent (5.979(4) and 6.106(4) Å). The interchain closest $\text{Co} \cdots \text{Co}$ distances were much longer (≥ 9 Å) than the intrachain ones, implying that the interchain magnetic interaction were negligible.

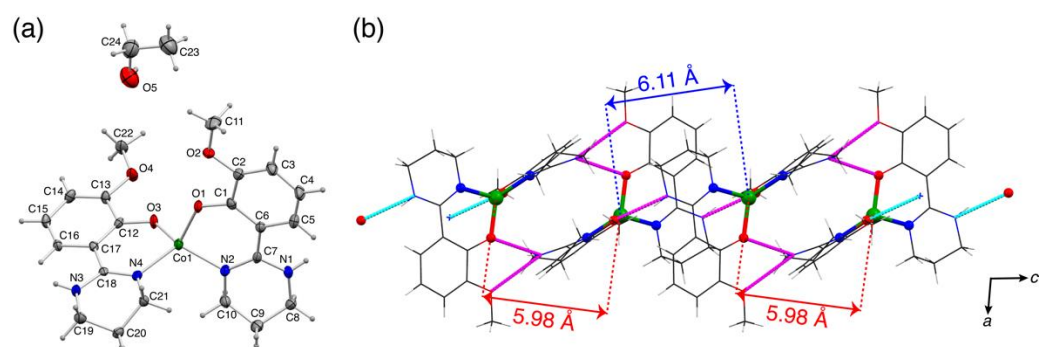


Figure 1. (a) Molecular structure of 1·C₂H₅OH (50% probability levels). (b) Hydrogen-bonded networks of 1·C₂H₅OH along *c* axis.

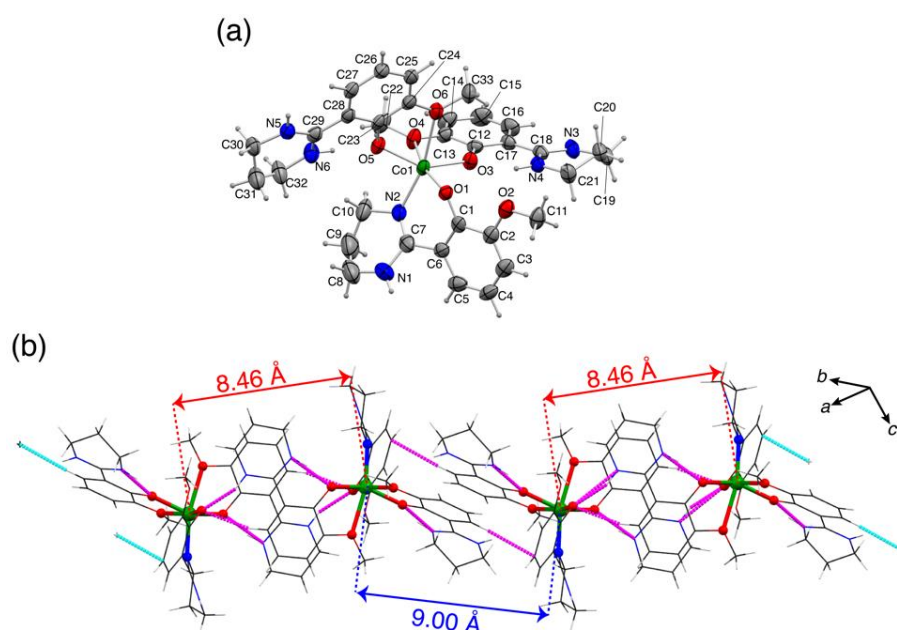


Figure 2. (a) Molecular structure of 2⁺ in 2BF₄·1.5C₂H₅OH (50% probability levels). (b) One-dimensional networks of 2⁺ by hydrogen-bond and N-H...π interactions.

Table 1. Selected bond parameters for 1·C₂H₅OH.

| Atom-Atom | Length/Å | Atom-Atom-Atom | Angle/° |
|------------|----------|-----------------|------------|
| Co(1)-O(1) | 1.913(2) | O(1)-Co(1)-N(2) | 94.08(10) |
| Co(1)-O(3) | 1.910(2) | O(3)-Co(1)-N(4) | 93.27(10) |
| Co(1)-N(2) | 1.982(3) | O(1)-Co(1)-O(3) | 106.28(10) |
| Co(1)-N(4) | 1.972(3) | O(1)-Co(1)-N(4) | 126.84(10) |
| | | O(3)-Co(1)-N(2) | 125.07(11) |
| | | N(2)-Co(1)-N(4) | 114.22(11) |

The 2BF₄ was crystallized in a triclinic system $P\bar{1}$ as 2BF₄·1.5C₂H₅OH (Figure 2). The hexa-coordinated geometry of the Co center was severely distorted by a NO₅ coordination mode. In 2⁺ cation, the Co center was coordinated by one Hmthp[−] and two H₂mthp ligands. Hmthp[−] acted as a bidentate ligand with phenolato-*O* atom and imino-*N* atoms as donor atoms, as was also observed in **1**, whereas H₂mthp ligands coordinated via phenolato-*O* and methoxy-*O* atoms in zwitterionic form, as observed in the crystal of H₂mthp. The protonation state of the ligands was consistent with the stoichiometry of the reaction condition (H₂mthp:KO^{*t*}Bu = 3:1). The coordination bonds with methoxy-*O* atoms were significantly longer than those with the other donor atoms (by 0.3 Å), implying the

weak coordination of the methoxy-O atoms. The bond parameters of Co ion were within the range of a typical divalent high-spin cobalt(II) complex (Table 2). The considerable distortion of the coordination geometry can be explained by the severe steric requirement of the six-membered chelate mode of the ligand in an octahedral geometry. The mean plane angles between the phenyl and tetrahydropyrimidinyl 6-membered rings of a Hmthp[−] ligand was 38.6(3)°, indicating that the ligand underwent a strong steric hindrance on O-N chelate mode in an octahedral coordination geometry [24]. It was noted that such distortion of the ligand was not observed in **1** because a tetrahedral coordination geometry accepted much larger bite angles than an octahedral one (109.5° for tetrahedral and 90° for octahedral geometry) and, the mean plane angles observed in **1** (15.4(3)° and 5.5(2)°) were comparable to those of H₂mthp. As a result, the bite angle of the six-membered chelate mode (phenolato- and imino-N atoms) in **2**⁺ was restricted to 91.44(14)°, although the angle of the five-membered chelate rings (phenolato-O and methoxy) accepted much smaller bite angles (72.58(11)° or 71.15(12)°). Although one-dimensional chain networks were formed by hydrogen-bond and N-H⋯π interactions, the shortest Co⋯Co distance was not the intrachain one but the interchain one (8.239(1) Å). This long intermolecular Co⋯Co distance suggested that the intermolecular magnetic interaction was negligible.

Table 2. Selected bond parameters for 2BF₄·1.5C₂H₅OH.

| Atom-Atom | Length/Å | Atom-Atom-Atom | Angle/° |
|------------|----------|-----------------|------------|
| Co(1)-O(1) | 2.002(3) | O(1)-Co(1)-N(2) | 91.44(14) |
| Co(1)-O(3) | 1.982(3) | O(3)-Co(1)-O(4) | 72.58(11) |
| Co(1)-O(4) | 2.354(3) | O(5)-Co(1)-O(6) | 71.15(12) |
| Co(1)-O(5) | 1.998(3) | O(1)-Co(1)-O(3) | 90.51(11) |
| Co(1)-O(6) | 2.387(3) | O(1)-Co(1)-O(5) | 108.44(12) |
| Co(1)-N(2) | 2.041(4) | O(1)-Co(1)-O(6) | 91.16(11) |
| | | N(2)-Co(1)-O(3) | 111.63(15) |
| | | N(2)-Co(1)-O(4) | 92.64(14) |
| | | N(2)-Co(1)-O(5) | 93.62(14) |
| | | O(3)-Co(1)-O(6) | 83.54(12) |
| | | O(4)-Co(1)-O(5) | 87.83(12) |
| | | O(1)-Co(1)-O(4) | 162.93(11) |
| | | N(2)-Co(1)-O(6) | 164.58(13) |
| | | O(3)-Co(1)-O(5) | 148.22(14) |
| | | O(4)-Co(1)-O(6) | 89.29(12) |

2.3. Magnetic Properties

2.3.1. Static Magnetic Properties

The temperature dependence of magnetic susceptibility was measured for **1**·C₂H₅OH and 2BF₄·1.5C₂H₅OH to reveal their magnetic properties (Figure 3). The $\chi_M T$ product at 300 K for **1**·C₂H₅OH (ca. 2.5 cm³ mol^{−1} K), which was higher than the spin-only value 1.876 for the *S* = 3/2 system, was a typical value for tetrahedral cobalt(II) complexes. Upon cooling, the $\chi_M T$ products were almost constant, down to 100 K, followed by a steep drop of value because of ZFS. To determine the *g*-factors and the axial ZFS parameter (*D*), the temperature dependence of the $\chi_M T$ data and the field dependence of the magnetization were simultaneously fitted to the following spin Hamiltonian:

$$\hat{H} = g\beta H\hat{S} + D \left[\hat{S}_z^2 - \frac{S(S+1)}{3} \right] + zJ S_z \hat{S} \quad (1)$$

where β and *zJ* are Bohr magneton and the intermolecular interaction, respectively (Table 3). The transversal ZFS parameter (*E*) was not considered as it was difficult to determine from the magnetic data. Intermolecular magnetic interactions were considered for **1**·C₂H₅OH to analyze the effect of intermolecular coupling on the magnetic relaxation dynamics. Although Hmthp[−] was a derivative of the Hthp[−] ligand, with the same coordination mode,

the obtained g -factors for $1 \cdot \text{C}_2\text{H}_5\text{OH}$ were rather closer to those of $[\text{Co}(\text{Hmimn})_2] \cdot \text{CH}_3\text{OH}$ than $[\text{Co}(\text{Hthp})_2]$ [12,13]. This suggested that the electronic structure of the phenolate donor had stronger influence on the g -factors. The large negative D value, owing to the second order spin-orbit coupling, was suggestive of SIM behavior with a spin-reversal barrier of ca. 100 cm^{-1} ($2|D|$).

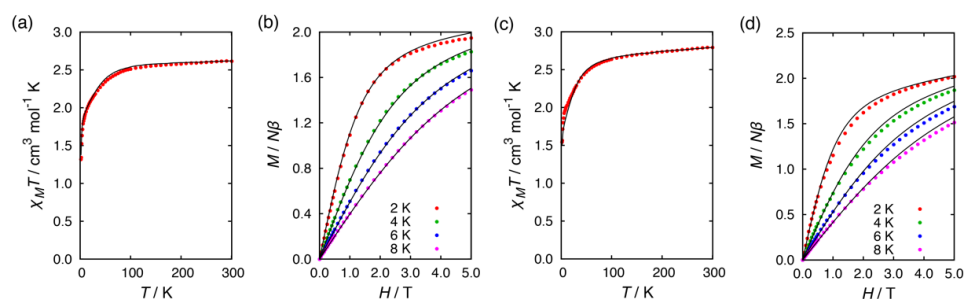


Figure 3. (a) Temperature dependence of $\chi_{\text{M}}T$ product for $1 \cdot \text{C}_2\text{H}_5\text{OH}$. (b) The field dependence of the magnetization at 2, 4, 6, and 8 K for $1 \cdot \text{C}_2\text{H}_5\text{OH}$. (c) Temperature dependence of $\chi_{\text{M}}T$ product for $2\text{BF}_4 \cdot 1.5\text{C}_2\text{H}_5\text{OH}$. (d) The field dependence of the magnetization at 2, 4, 6, and 8 K for $2\text{BF}_4 \cdot 1.5\text{C}_2\text{H}_5\text{OH}$. Solid lines correspond to the fit using the MagSakiTetra program.

Table 3. Experimental g -factors (g_x, g_y, g_z), axial ZFS parameters (D), intermolecular magnetic interactions (z), and temperature-independent paramagnetism (TIP).

| | $1 \cdot \text{C}_2\text{H}_5\text{OH}$ | $2\text{BF}_4 \cdot 1.5\text{C}_2\text{H}_5\text{OH}$ | $[\text{Co}(\text{Hthp})_2]^i$ | $[\text{Co}(\text{Hmimn})_2] \cdot \text{CH}_3\text{OH}^{ii}$ |
|-------------------------------------|---|---|--------------------------------|---|
| g_x, g_y | 2.16 | 2.35 | 2.18 | 2.18 |
| g_z | 2.56 | 2.42 | 2.48 | 2.55 |
| D/cm^{-1} | −49 | −31 | −30 | −30 |
| z/cm^{-1} | −0.56 | 0 | −1.5 | −0.25 |
| TIP/ $\text{cm}^3 \text{ mol}^{-1}$ | 0.0003 | 0.0005 | 0.0003 | 0.0003 |

ⁱ Hthp[−] = 2-(1,4,5,6-tetrahydropyrimidin-2-yl)phenolate [13]. ⁱⁱ Hmimn[−] = 2-(2-imidazolyl)-6-methoxyphenolate.

The $\chi_{\text{M}}T$ product for $2\text{BF}_4 \cdot 1.5\text{C}_2\text{H}_5\text{OH}$ (ca. $2.8 \text{ cm}^3 \text{ mol}^{-1} \text{ K}$) was also higher than the spin-only value because of unquenched orbital contribution on the magnetic moment. The simultaneous fitting of the $\chi_{\text{M}}T$ vs. T and M vs. H plots was performed. Intermolecular interaction was not considered, because the intermolecular Co \cdots Co distance was significantly long. The obtained zero-field splitting parameter D was negative and relatively small among octahedral Co^{II} SIMs, presumably due to severely distorted octahedral geometry [9,16,17].

2.3.2. Dynamic magnetic properties

Alternating current (ac) susceptibility measurements for $1 \cdot \text{C}_2\text{H}_5\text{OH}$ exhibited significant frequency dependence on the out-of-phase signal (χ_{M}'') in the absence of an external magnetic field at 1.9 K (Figure 4). This was indicative of slow magnetic relaxation in the absence of an external field. It should be noted that zero-field SIM behavior in a 3d metal complex is still very rare owing to fast relaxation via QTM. Upon heating, however, the χ_{M}'' vs. frequency plot showed no change except the weakening of the χ_{M}'' signal. This temperature independence is a characteristic feature of QTM. By applying an external field, on the other hand, another relaxation process appeared in the lower frequency region in the χ_{M}'' vs. frequency plot (Figures S3 and 4b). The temperature dependence was measured in the presence of 3.5 kOe, where the QTM relaxation pathway was completely suppressed and relatively small contribution of the direct relaxation process was expected. To elucidate the relaxation dynamics, the relaxation time τ was extracted by the generalized Debye-fit model:

$$\chi_{\text{ac}}(\omega) = \chi_{\text{S}} + \frac{\chi_{\text{T}} - \chi_{\text{S}}}{1 + (i\omega\tau)^{1-\alpha}} \quad (2)$$

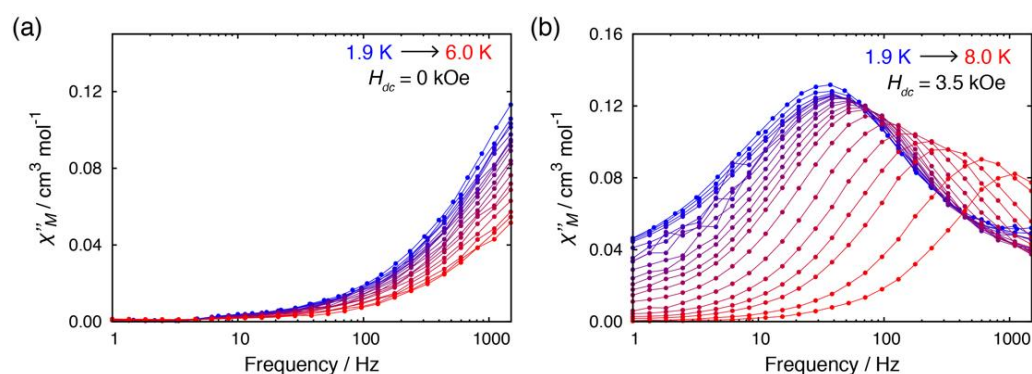


Figure 4. Temperature dependence of out-of-phase (χ_M'') susceptibilities for $1\text{-C}_2\text{H}_5\text{OH}$ (a) in the absence of the dc field and (b) in the presence of dc field ($H_{dc} = 3.5$ kOe). Lines are guide for the eyes.

The relaxation dynamics could not be fitted with a single relaxation process, as it showed different trends below and above ca. 4 K (Figure 5). The dynamics was nicely fitted with a combination of two processes, direct and Raman relaxation processes:

$$\tau^{-1} = AH^4T + CT^n \quad (3)$$

where A , C , and n are coefficients, H is the magnetic field, T is the temperature ($A = 0.667 \text{ K}^{-1} \text{ kOe}^{-4} \text{ s}^{-1}$, $C = 1.23 \times 10^{-1} \text{ s}^{-1} \text{ K}^{-5.2}$, $n = 5.2$). In the low temperature region (<4 K), the direct process, which involves relaxation from $-M_s$ to $+M_s$ with emission of a single lattice phonon, was the predominant relaxation process. This predominance could be elucidated by the presence of a relatively strong external field (3.5 kOe) as the τ was inversely proportional to the powers of an external field. Above 4 K, the relaxation dynamics were taken over by the Raman process, in which relaxation between $\pm M_s$ states occurred via virtual state. The n value should be ≤ 9 for a Kramers ion when both an acoustic and an optical phonon are considered, and the obtained n value for $1\text{-C}_2\text{H}_5\text{OH}$ was consistent with the expected value [25,26].

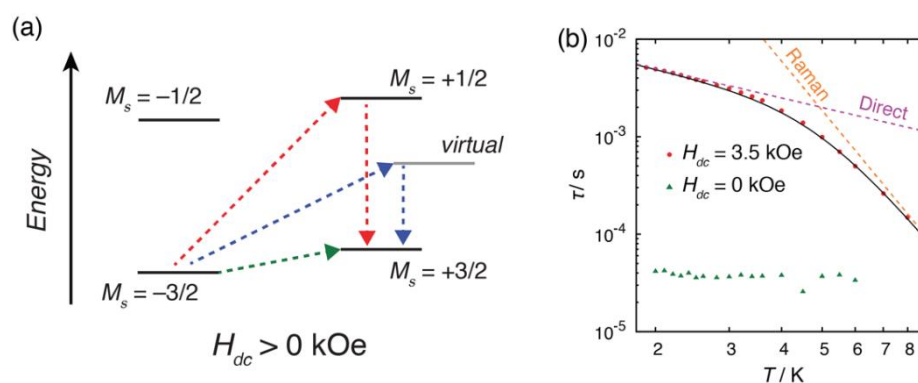


Figure 5. (a) Possible spin-lattice relaxation processes of the Co complexes under an external magnetic field. The red, blue and green arrows indicate Orbach, Raman and direct relaxation processes, respectively. (b) Temperature dependence of relaxation time τ . The dashed lines indicate fitted lines for a single relaxation process of Raman and direct process. The solid black lines indicate the sum of the relaxation processes.

As observed in previously reported three analogous compounds [12,13], $1\text{-C}_2\text{H}_5\text{OH}$ exhibited one-dimensional hydrogen-bonded networks as well as zero-field slow magnetic relaxation. We reported that the relatively short intermolecular $\text{Co}\cdots\text{Co}$ distance induced a static exchange bias field to split the ground $\pm M_s$ levels. As this splitting of the ground $\pm M_s$ levels effectively suppressed the QTM phenomena, formation of hydrogen-bonded networks was a feasible approach for zero-field SIMs. In the case of one-dimensional chain,

the efficiency of suppression of QTM was dependent on the molecular orientation and symmetry of the alignment of the chain. As the Co centers in the chain structures were antiferromagnetically coupled, alternating spin orientation should be the ground state. In this state, QTM would be suppressed, because the two neighboring molecules in a chain induced a dipolar field to split the ground $\pm M_s$ levels. When the dipolar field of the two neighboring molecules were stochastically oriented to opposite direction, on the other hand, the dipolar field would be canceled and QTM could not be suppressed, as observed in $[\text{Co}(\text{Hthp})_2]$ ($\text{Himn}^- = 2\text{-}(1,4,5,6\text{-tetrahydropyrimidin-2-yl})\text{phenolate}$). This was not the case when the two intrachain $\text{Co}\cdots\text{Co}$ distances were significantly different because the dipolar field from the two neighboring molecules would not be canceled, as observed in $[\text{Co}(\text{Himn})_2]$ ($\text{Himn}^- = 2\text{-}(2\text{-imidazolyl})\text{phenolate}$). In $1\cdot\text{C}_2\text{H}_5\text{OH}$, two intrachain distances were slightly different (ca. 0.1 Å) but the difference was only half the value of $[\text{Co}(\text{Himn})_2]$. Consequently, the dipolar field was almost canceled, and the QTM was only partially suppressed in the absence of an external field. These results indicated that the difference in the intrachain $\text{Co}\cdots\text{Co}$ distances was an important factor to suppress the QTM as well as the intermolecular magnetic coupling.

Ac susceptibility measurement was also performed on complex $2\text{BF}_4\cdot 1.5\text{C}_2\text{H}_5\text{OH}$. Unlike $1\cdot\text{C}_2\text{H}_5\text{OH}$, this complex did not exhibit slow magnetic relaxation in the absence of an external magnetic field, presumably because the $\text{Co}\cdots\text{Co}$ distance in $2\text{BF}_4\cdot 1.5\text{C}_2\text{H}_5\text{OH}$ was not short enough to cause intermolecular magnetic coupling to suppress the QTM (Figure S6). In the presence of a magnetic field, on the other hand, QTM was well suppressed, meaning that 2^+ cation was a field-induced SIM (Figure 6). To investigate the relaxation dynamics, temperature dependence of the ac susceptibility was measured under a static field of 1.0 kOe. The τ vs. T plot suggested that there were two relaxation processes present and they switched at ca. 4 K. Below 4 K, the double-logarithmic plot showed a large degree of linearity suggesting a power law ($\tau \propto T^{-n}$). The relaxation dynamics was well-fitted by combining the Raman and Orbach relaxation processes:

$$\tau^{-1} = CT^n + \tau_0^{-1} \exp\left(\frac{\Delta_{\text{Orbach}}}{k_B T}\right) \quad (4)$$

where τ_0 is the pre-exponential factor, Δ_{Orbach} is the relaxation barrier, and k_B is the Boltzmann constant ($C = 45.5 \text{ s}^{-1} \text{ K}^{-2.6}$, $n = 2.6$, $\tau_0 = 2.45 \times 10^{-9} \text{ s}$, $\Delta_{\text{Orbach}} = 36.7 \text{ cm}^{-1}$). The n value was within the range of expected value for the Raman process. It was noted that the combination of the phonon-bottlenecked direct process (low temperature region) and the Raman process (high temperature region) did not give a reasonable fit. The relaxation barrier for the Orbach process Δ_{Orbach} was slightly smaller than the expected value from the ZFS parameter $2|D|$. Thus, the relaxation dynamics of high-temperature region of $2\text{BF}_4\cdot 1.5\text{C}_2\text{H}_5\text{OH}$ were dominated by the Orbach process.

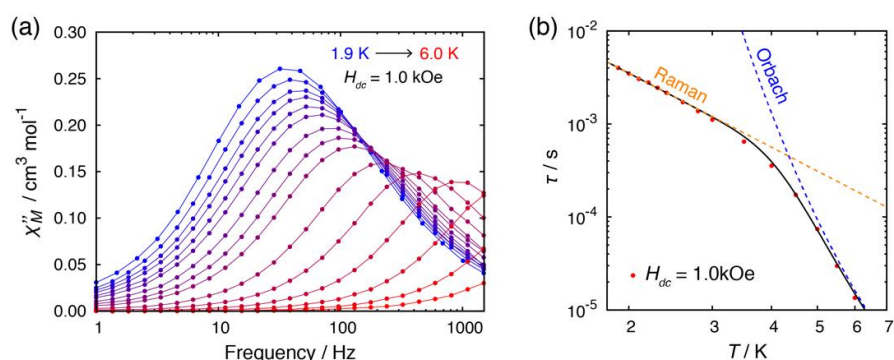


Figure 6. (a) Temperature dependence of out-of-phase (χ_M'') susceptibilities for $2\text{BF}_4\cdot 1.5\text{C}_2\text{H}_5\text{OH}$ in the presence of dc field ($H_{dc} = 1.0 \text{ kOe}$). Lines are guide for the eyes. (b) Temperature dependence of relaxation time τ . The dashed lines indicate fitted lines for a single relaxation process of Raman and Orbach process. The solid black lines indicate the sum of the relaxation processes.

3. Materials and Methods

3.1. General Consideration

All the chemicals were used as received without further purification, except for $\text{Co}(\text{BF}_4)_2 \cdot 6\text{H}_2\text{O}$, which was recrystallized from a water/ethanol mixed solvent before use. Elemental analyses (C, H, and N) were performed at the Research Institute for Instrumental Analysis, Kanazawa University. ^1H NMR measurements were carried out at 22°C on a JEOL 400SS spectrometer. Chemical shifts were referenced to the solvent residual peak [27]. Infrared spectra were measured on a JASCO FT/IR-4200 spectrometer.

3.2. Preparations

2-(1,4,5,6-tetrahydropyrimidin-2-yl)-6-methoxyphenol (H_2mthp). A mixture of methyl 3-methoxysalicylate (9.11 g, 50 mmol) and 1,3-diaminopropane (12 mL) was refluxed overnight. The unreacted 1,3-diaminopropane was evaporated off under ambient pressure, followed by the addition of 5 mL ethanol. After cooling, the yellowish residue was collected by filtration and washed with ethanol. Yield: 7.02 g, 68%. ^1H NMR (399 MHz, Methanol- d_4) δ 7.02 (d, $J = 8.8$ Hz, 1H, aryl-H), 6.83 (d, $J = 7.7$ Hz, 1H, aryl-H), 6.45–6.38 (m, 1H, aryl-H), 3.78 (s, 3H, $-\text{CH}_3$), 3.59–3.46 (m, 4H, $-\text{CH}_2-$), 2.02 (quin, $J = 5.8$ Hz, 2H, $-\text{CH}_2-$).

$[\text{Co}(\text{Hmthp})_2] \cdot \text{C}_2\text{H}_5\text{OH}$ ($1 \cdot \text{C}_2\text{H}_5\text{OH}$). An ethanol solution (10 mL) of $\text{Co}(\text{BF}_4)_2 \cdot 6\text{H}_2\text{O}$ (34.1 mg, 0.10 mmol) was slowly added to a mixture of ethanol (10 mL), H_2mthp (62.0 mg, 0.30 mmol) and KO^tBu (23.0 mg, 0.20 mmol) in a Schlenk flask under Ar atmosphere. The reaction mixture was allowed to stand at room temperature for a few days, and red crystals were obtained. Yield: 11.3 mg, 22%. The crystallinity of this compound was easily lost in air, due to its efflorescent nature, and solvent molecules of crystallization were substituted by water. Anal Calcd for $[\text{Co}(\text{Hmthp})_2] \cdot 0.7\text{H}_2\text{O} = \text{C}_{22}\text{H}_{27}\text{CoN}_4\text{O}_{4.7}$: C, 54.82; H, 5.73; N, 11.62%. Found: C, 54.64; H, 5.58; N, 11.62%.

$[\text{Co}(\text{Hmthp})(\text{H}_2\text{mthp})_2]\text{BF}_4 \cdot 1.5\text{C}_2\text{H}_5\text{OH}$ ($2\text{BF}_4 \cdot 1.5\text{C}_2\text{H}_5\text{OH}$). An ethanol solution (5 mL) of $\text{Co}(\text{BF}_4)_2 \cdot 6\text{H}_2\text{O}$ (35.0 mg, 0.10 mmol) was slowly added to a mixture of ethanol (5 mL), H_2mthp (62.2 mg, 0.30 mmol) and KO^tBu (10.4 mg, 0.09 mmol) in a Schlenk flask under Ar atmosphere. The reaction mixture was allowed to stand at room temperature for a few weeks, and purple crystals were obtained. Yield: 46.9 mg, 61%. The crystallinity of this compound was easily lost in air, due to its efflorescent nature, and solvent molecules of crystallization were substituted by water. Anal Calcd for $[\text{Co}(\text{Hmthp})(\text{H}_2\text{mthp})_2]\text{BF}_4 \cdot 2\text{H}_2\text{O} = \text{C}_{33}\text{H}_{45}\text{BCoF}_4\text{N}_6\text{O}_8$: C, 49.58; H, 5.67; N, 10.51%. Found: C, 49.59; H, 5.76; N, 10.08%.

3.3. Crystallography

Crystallographic data are summarized in Table 4. Single-crystal X-ray diffraction data were obtained with a Rigaku XtaLAB AFC11 diffractometer with graphite-monochromated $\text{Mo K}\alpha$ radiation ($\lambda = 0.71073 \text{ \AA}$). A single crystal was mounted with a glass capillary and flash-cooled with a cold N_2 gas stream. Data were processed using the CrysAlisPro software packages. The structures were solved by intrinsic phasing methods using the SHELXT [28] software packages, and refined on F_2 (with all independent reflections) using the SHELXL [29] software packages. The non-hydrogen atoms were refined anisotropically. In $2\text{BF}_4 \cdot 1.5\text{C}_2\text{H}_5\text{OH}$, a BF_4^- anion and ethanol molecules of crystallization were disordered at two possible positions. The rigid-bond restraint (RIGU) and SIMU command were employed for these disordered atoms except for one of two parts of BF_4^- anion (B1, F1, F2, F3, and F4). All B-F bonds were restrained to the same distances by the SADI command. The C-O bonds for ethanol molecules and B-F bonds for the minor part of BF_4^- (B2, F5, F6, F7, and F8) were constrained by the DFIX command. The DANG command was employed to restrain C-C-O angles of the ethanol molecules.

Table 4. Crystallographic data and refinement parameters of **1**, **2BF₄·1.5C₂H₅OH** and **H₂mthp**.

| Complex | 1·C₂H₅OH | 2BF₄·1.5C₂H₅OH | H₂mthp |
|---|---|---|---|
| Empirical formula | C ₂₄ H ₃₂ CoN ₄ O ₅ | C ₃₆ H ₅₀ BCoF ₄ N ₆ O _{7.5} | C ₁₁ H ₁₄ N ₂ O ₂ |
| Formula weight | 515.46 | 832.56 | 206.24 |
| Crystal system | Monoclinic | Triclinic | Orthorhombic |
| Crystal dimensions/mm | 0.08 × 0.05 × 0.02 | 0.15 × 0.09 × 0.07 | 0.16 × 0.11 × 0.07 |
| Space group | <i>P</i> 2 ₁ / <i>c</i> | <i>P</i> $\bar{1}$ | <i>P</i> 2 ₁ 2 ₁ 2 ₁ |
| <i>a</i> /Å | 10.3216(6) | 12.1036(6) | 7.5402(2) |
| <i>b</i> /Å | 19.6289(11) | 13.6859(6) | 12.0806(3) |
| <i>c</i> /Å | 11.8343(6) | 13.9026(8) | 22.6040(8) |
| α /° | | 114.527(5) | |
| β /° | 96.137(5) | 104.484(4) | |
| γ /° | | 92.660(4) | |
| <i>V</i> /Å ³ | 2383.9(2) | 1998.83(19) | 2059.00(10) |
| <i>Z</i> | 4 | 2 | 8 |
| <i>T</i> /K | 100(2) | 100(2) | 100(2) |
| ρ_{calcd} /g·cm ⁻³ | 1.436 | 1.383 | 1.331 |
| μ /mm ⁻¹ | 0.763 | 0.503 | 0.093 |
| <i>F</i> (000) | 1084 | 872 | 880 |
| 2 θ_{max} /° | 55 | 55 | 55 |
| No. of reflections measured | 20466 | 26576 | 12996 |
| No. of independent reflections | 5452 (<i>R</i> _{int} = 0.0866) | 9145 (<i>R</i> _{int} = 0.0482) | 4588 (<i>R</i> _{int} = 0.0339) |
| Data/restraints/parameters | 5452/0/319 | 9145/83/552 | 4588/4/289 |
| <i>R</i> ₁ [<i>I</i> > 2.00 σ (<i>I</i>)] ⁱ | 0.0621 | 0.0852 | 0.0376 |
| <i>wR</i> ₂ (all reflections) ⁱⁱ | 0.1230 | 0.2784 | 0.0850 |
| Goodness of fit indicator | 1.043 | 1.040 | 1.030 |
| Highest peak, deepest hole/e Å ⁻³ | 0.437, -0.575 | 1.432, -0.799 | 0.181, -0.214 |
| CCDC deposition number | 2216987 | 2216988 | 2216989 |

$$^i R_1 = \sum ||F_o| - |F_c|| / \sum |F_o|, ^{ii} wR_2 = [\sum (w(F_o^2 - F_c^2)^2) / \sum w(F_o^2)^2]^{1/2}.$$

3.4. Magnetic Measurements

Magnetic susceptibility measurements were performed with a MPMS-7 or MPMS-XL7 SQUID magnetometer. Susceptibility data were recorded in the temperature range from 1.9 to 300 K with a static field of 5.0 kOe. The polycrystalline samples were grounded into fine powders by an agate mortar in dried condition. The samples were loaded into a gelatin capsule and covered in liquid paraffin to prevent field-induced orientation of crystals. All data were corrected for diamagnetism of the sample by means of Pascal's constants [30]. Temperature dependence of the magnetic susceptibility and field dependence of the magnetization data were fitted using the MagSakiTetra W0913 program [31]. The dynamic susceptibility was measured with alternating-current (ac) fields of 3 Oe magnitude and a constant direct current (dc) field of 0–4.0 kOe in the frequency range from 1 to 1500 Hz. The relaxation time τ was extracted from fitting to the generalized Debye model. The fit was performed using the CC-Fit program [32].

4. Conclusions

In this study, tetra-coordinated and a hexa-coordinated Co^{II} complexes, containing the same ligand, were prepared and characterized by X-ray crystallography and magnetometry. In the crystal, the tetracoordinated complex **1·C₂H₅OH** possessed pseudo-tetrahedral coordination geometry and formed one-dimensional chain networks by intermolecular hydrogen-bonding interactions. Two intrachain Co···Co distances were slightly different (ca. 0.1 Å) and were short enough to induce a weak intermolecular magnetic coupling. Zero-field SIM behavior was observed for **1·C₂H₅OH** because QTM was partially suppressed by the non-zero intermolecular magnetic coupling. The partial suppression of QTM indicated that the difference in intrachain Co···Co distances is important to suppress QTM completely. On the other hand, the hexacoordinated complex **2BF₄·1.5C₂H₅OH** exhibited a severely distorted octahedral coordination geometry with one-dimensional networks by N-H··· π and hydrogen-bonding interactions. The intermolecular Co···Co distances were above the range of intermolecular magnetic coupling, and SIM behavior was observed only in the presence of an external field. Thus, these results indicated that not only non-zero

magnetic coupling, but also the difference of intrachain distances are important to achieve zero-field SIM.

Supplementary Materials: The following supporting information can be downloaded at: <https://www.mdpi.com/article/10.3390/magnetochemistry9010017/s1>. Figure S1: Molecular structure of H₂mthp (50% probability levels); Figure S2: Temperature dependence of (a) the in-phase χ_M' vs. frequency plots and (b) out-of-phase χ_M'' vs. frequency plots for 1·C₂H₅OH in the absence of a dc field with ac frequency of 1–1488 Hz; Figure S3: Dc field dependence of (a) the in-phase χ_M' vs. frequency plots and (b) out-of-phase χ_M'' vs. frequency plots for 1·C₂H₅OH at 1.9 K with ac frequency of 1–1488 Hz; Figure S4: Temperature dependence of (a) the in-phase χ_M' vs. frequency plots and (b) out-of-phase χ_M'' vs. frequency plots for 1·C₂H₅OH in the presence of 3.5 kOe with ac frequency of 1–1488 Hz; Figure S5: Cole–Cole plot for 1·C₂H₅OH (a) in the absence and (b) in the presence of 3.5 kOe dc field; Figure S6: Dc field dependence of (a) the in-phase χ_M' vs. frequency plots and (b) out-of-phase χ_M'' vs. frequency plots for 2·1.5C₂H₅OH at 1.9 K with ac frequency of 1–1488 Hz; Figure S7: Temperature dependence of (a) the in-phase χ_M' vs. frequency plots and (b) out-of-phase χ_M'' vs. frequency plots for 2·1.5C₂H₅OH in the presence of 1.0 kOe with ac frequency of 1–1488 Hz; Figure S8. Cole–Cole plot for 2·1.5C₂H₅OH in the presence of 1.0 kOe dc field; Table S1: Hydrogen-bond distances and angles; Table S2: Cole–Cole fit values for 1·C₂H₅OH in 3.5 kOe dc field from 1.9 to 8.0 K; Table S3: Cole–Cole fit values for 1·C₂H₅OH in 0 kOe dc field from 1.9 to 6.0 K; Table S4. Cole–Cole fit values for 2BF₄·1.5C₂H₅OH in 1.0 kOe dc field from 1.9 to 6.0 K. Figure S9. ¹H NMR spectrum of H₂mthp in CD₃OD. Figure S10. Infrared spectra of (a) pristine 1·C₂H₅OH, (b) hydrated 1·C₂H₅OH, (c) pristine 2BF₄·1.5C₂H₅OH, (d) hydrated 2BF₄·1.5C₂H₅OH, and H₂mthp (nujol mull).

Author Contributions: Conceptualization, R.M.; methodology, R.M.; investigation, R.M. and H.S.; resources, R.M. and Y.H.; writing—original draft, R.M.; writing—review and editing, R.M., H.S. and Y.H.; visualization, R.M. project administration, R.M. All authors have read and agreed to the published version of the manuscript.

Funding: This work was partly funded by a Grant-in-Aid for Scientific Research No. 19K15525 from MEXT, Japan. This work was partially supported by The Mitani Foundation for Research and Development.

Data Availability Statement: The crystallographic data are available from the Cambridge Crystallographic Data Centre (CCDC). Other data not presented in Supplementary Materials are available on request from the corresponding author.

Acknowledgments: We thank Yuya Imai (Kanazawa University) for ¹H NMR measurement. A part of this work was conducted in the Institute for Molecular Science, supported by the Advanced Research Infrastructure for Materials and Nanotechnology (JPMXP1222MS1013 and JPMXP1222MS1013b of the Ministry of Education, Culture, Sports, Science and Technology (MEXT), Japan.

Conflicts of Interest: The authors declare no conflict of interest.

References

1. Sessoli, R.; Gatteschi, D.; Caneschi, A.; Novak, M.A. Magnetic bistability in a metal-ion cluster. *Nature* **1993**, *365*, 141–143. [[CrossRef](#)]
2. Mannini, M.; Pineider, F.; Sainctavit, P.; Danieli, C.; Otero, E.; Sciancalepore, C.; Talarico, A.M.; Arrio, M.-A.; Cornia, A.; Gatteschi, D.; et al. Magnetic memory of a single-molecule quantum magnet wired to a gold surface. *Nat. Mater.* **2009**, *8*, 194–197. [[CrossRef](#)] [[PubMed](#)]
3. Ardavan, A.; Rival, O.; Morton, J.J.L.; Blundell, S.J.; Tyryshkin, A.M.; Timco, G.A.; Winpenny, R.E.P. Will Spin-Relaxation Times in Molecular Magnets Permit Quantum Information Processing? *Phys. Rev. Lett.* **2007**, *98*, 057201. [[CrossRef](#)] [[PubMed](#)]
4. Stamp, P.C.E.; Gaita-Ariño, A. Spin-based quantum computers made by chemistry: Hows and whys. *J. Mater. Chem.* **2009**, *19*, 1718–1730. [[CrossRef](#)]
5. Gaita-Ariño, A.; Luis, F.; Hill, S.; Coronado, E. Molecular spins for quantum computation. *Nat. Chem.* **2019**, *11*, 301–309. [[CrossRef](#)] [[PubMed](#)]
6. Ishikawa, N.; Sugita, M.; Ishikawa, T.; Koshihara, S.Y.; Kaizu, Y. Lanthanide double-decker complexes functioning as magnets at the single-molecular level. *J. Am. Chem. Soc.* **2003**, *125*, 8694–8695. [[CrossRef](#)] [[PubMed](#)]
7. Harman, W.H.; Harris, T.D.; Freedman, D.E.; Fong, H.; Chang, A.; Rinehart, J.D.; Ozarowski, A.; Sougrati, M.T.; Grandjean, F.; Long, G.J.; et al. Slow Magnetic Relaxation in a Family of Trigonal Pyramidal Iron(II) Pyrrolide Complexes. *J. Am. Chem. Soc.* **2010**, *132*, 18115–18126. [[CrossRef](#)]

8. Rechkemmer, Y.; Breitgoff, F.D.; van der Meer, M.; Atanasov, M.; Hakl, M.; Orlita, M.; Neugebauer, P.; Neese, F.; Sarkar, B.; van Slageren, J. A four-coordinate cobalt(II) single-ion magnet with coercivity and a very high energy barrier. *Nat. Commun.* **2016**, *7*, 10467. [[CrossRef](#)]
9. Mitsuhashi, R.; Pedersen, K.S.; Ueda, T.; Suzuki, T.; Bendix, J.; Mikuriya, M. Field-induced single-molecule magnet behavior in ideal trigonal antiprismatic cobalt(II) complexes: Precise geometrical control by a hydrogen-bonded rigid metalloligand. *Chem. Commun.* **2018**, *54*, 8869–8872. [[CrossRef](#)]
10. Mitsuhashi, R.; Hosoya, S.; Sunatsuki, Y.; Suzuki, T.; Mikuriya, M. Field-induced single-ion magnet behaviors in 1-dimensionally assembled tetrahedral cobalt(II) complexes with halide donors. *Inorg. Chim. Acta* **2022**, *529*, 120667. [[CrossRef](#)]
11. Zadrozny, J.M.; Long, J.R. Slow magnetic relaxation at zero field in the tetrahedral complex $[\text{Co}(\text{SPh})_4]^{2-}$. *J. Am. Chem. Soc.* **2011**, *133*, 20732–20734. [[CrossRef](#)]
12. Mitsuhashi, R.; Hosoya, S.; Suzuki, T.; Sunatsuki, Y.; Sakiyama, H.; Mikuriya, M. Hydrogen-bonding interactions and magnetic relaxation dynamics in tetracoordinated cobalt(II) single-ion magnets. *Dalton Trans.* **2019**, *48*, 395–399. [[CrossRef](#)] [[PubMed](#)]
13. Mitsuhashi, R.; Hosoya, S.; Suzuki, T.; Sunatsuki, Y.; Sakiyama, H.; Mikuriya, M. Zero-field slow relaxation of magnetization in cobalt(II) single-ion magnets: Suppression of quantum tunneling of magnetization by tailoring the intermolecular magnetic coupling. *RSC Adv.* **2020**, *10*, 43472–43479. [[CrossRef](#)] [[PubMed](#)]
14. da Cunha, T.T.; Barbosa, V.M.M.; Oliveira, W.X.C.; Pedroso, E.F.; García, D.M.A.; Nunes, W.C.; Pereira, C.L.M. Field-Induced Slow Magnetic Relaxation of a Six-Coordinate Mononuclear Manganese(II) and Cobalt(II) Oxamate Complexes. *Inorg. Chem.* **2020**, *59*, 12983–12987. [[CrossRef](#)]
15. Yao, B.; Singh, M.K.; Deng, Y.-F.; Wang, Y.-N.; Dunbar, K.R.; Zhang, Y.-Z. Trigonal Prismatic Cobalt(II) Single-Ion Magnets: Manipulating the Magnetic Relaxation Through Symmetry Control. *Inorg. Chem.* **2020**, *59*, 8505–8513. [[CrossRef](#)] [[PubMed](#)]
16. Saber, M.R.; Singh, M.K.; Dunbar, K.R. Geometrical control of the magnetic anisotropy in six coordinate cobalt complexes. *Chem. Commun.* **2020**, *56*, 8492–8495. [[CrossRef](#)] [[PubMed](#)]
17. Deng, Y.-F.; Singh, M.K.; Gan, D.; Xiao, T.; Wang, Y.; Liu, S.; Wang, Z.; Ouyang, Z.; Zhang, Y.-Z.; Dunbar, K.R. Probing the Axial Distortion Effect on the Magnetic Anisotropy of Octahedral Co(II) Complexes. *Inorg. Chem.* **2020**, *59*, 7622–7630. [[CrossRef](#)]
18. Wernsdorfer, W.; Aliaga-Alcalde, N.; Hendrickson, D.N.; Christou, G. Exchange-biased quantum tunnelling in a supramolecular dimer of single-molecule magnets. *Nature* **2002**, *416*, 406–409. [[CrossRef](#)]
19. Hill, S.; Edwards, R.S.; Aliaga-Alcalde, N.; Christou, G. Quantum Coherence in an Exchange-Coupled Dimer of Single-Molecule Magnets. *Science* **2003**, *302*, 1015–1018. [[CrossRef](#)]
20. Nguyen, T.N.; Wernsdorfer, W.; Abboud, K.A.; Christou, G. A supramolecular aggregate of four exchange-biased single-molecule magnets. *J. Am. Chem. Soc.* **2011**, *133*, 20688–20691. [[CrossRef](#)]
21. Han, T.; Giansiracusa, M.J.; Li, Z.H.; Ding, Y.S.; Chilton, N.F.; Winpenny, R.E.P.; Zheng, Y.Z. Exchange-Biasing in a Dinuclear Dysprosium(III) Single-Molecule Magnet with a Large Energy Barrier for Magnetisation Reversal. *Chem.—A Eur. J.* **2020**, *26*, 6773–6777. [[CrossRef](#)] [[PubMed](#)]
22. Mitsuhashi, R.; Suzuki, T.; Sunatsuki, Y. Four-Electron Oxidative Dehydrogenation Induced by Proton-Coupled Electron Transfer in Ruthenium(III) Complex with 2-(1,4,5,6-Tetrahydropyrimidin-2-yl)phenolate. *Inorg. Chem.* **2013**, *52*, 10183–10190. [[CrossRef](#)] [[PubMed](#)]
23. Yang, L.; Powell, D.R.; Houser, R.P. Structural variation in copper(I) complexes with pyridylmethylamide ligands: Structural analysis with a new four-coordinate geometry index, τ_4 . *Dalton Trans.* **2007**, *36*, 955–964. [[CrossRef](#)]
24. Mitsuhashi, R.; Suzuki, T.; Hosoya, S.; Mikuriya, M. Hydrogen-Bonded Supramolecular Structures of Cobalt(III) Complexes with Unsymmetrical Bidentate Ligands: *mer/fac* Interconversion Induced by Hydrogen-Bonding Interactions. *Cryst. Growth Des.* **2017**, *17*, 207–213. [[CrossRef](#)]
25. Scott, P.L.; Jeffries, C.D. Spin-lattice relaxation in some rare-earth salts at helium temperatures; observation of the phonon bottleneck. *Phys. Rev.* **1962**, *127*, 32–51. [[CrossRef](#)]
26. Shrivastava, K. Theory of Spin–Lattice Relaxation. *Phys. Status Solidi B* **1983**, *117*, 437. [[CrossRef](#)]
27. Gottlieb, H.E.; Kotlyar, V.; Nudelman, A. NMR Chemical Shifts of Common Laboratory Solvents as Trace Impurities. *J. Org. Chem.* **1997**, *62*, 7512–7515. [[CrossRef](#)]
28. Sheldrick, G.M. SHELXT—Integrated space-group and crystal-structure determination. *Acta Crystallogr. Sect. A Found. Adv.* **2015**, *71*, 3–8. [[CrossRef](#)]
29. Sheldrick, G.M. Crystal structure refinement with SHELXL. *Acta Crystallogr. Sect. C Struct. Chem.* **2015**, *71*, 3–8. [[CrossRef](#)]
30. Bain, G.A.; Berry, J.F. Diamagnetic Corrections and Pascal’s Constants. *J. Chem. Educ.* **2008**, *85*, 532–536. [[CrossRef](#)]
31. Sakiyama, H. Development of MagSaki(Tetra) Software for the Magnetic Analysis of Tetranuclear High-spin Cobalt(II) Complexes. *J. Comput. Chem. Jpn.-Int. Ed.* **2016**, *2*, 2016-0001. [[CrossRef](#)]
32. Chilton, N.F. *CC-Fit*; The University of Manchester: Manchester, UK, 2014; Available online: <http://www.nfchilton.com/cc-fit.html> (accessed on 4 November 2019).

Disclaimer/Publisher’s Note: The statements, opinions and data contained in all publications are solely those of the individual author(s) and contributor(s) and not of MDPI and/or the editor(s). MDPI and/or the editor(s) disclaim responsibility for any injury to people or property resulting from any ideas, methods, instructions or products referred to in the content.